Article

Metal/Semiconductor Barrier Properties of Non-Recessed Ti/Al/Ti and Ta/Al/Ta Ohmic Contacts on AlGaN/GaN Heterostructures

Monia Spera [1,2,3,*], Giuseppe Greco [1,*], Raffaella Lo Nigro [1], Silvia Scalese [1], Corrado Bongiorno [1], Marco Cannas [3], Filippo Giannazzo [1] and Fabrizio Roccaforte [1]

[1] Consiglio Nazionale delle Ricerche—Istituto per la Microelettronica e Microsistemi (CNR-IMM), Strada VIII, n. 5, Zona Industriale, 95121 Catania, Italy

[2] Department of Physics and Astronomy, University of Catania, Via Santa Sofia, 64, 95123 Catania, Italy

[3] Department of Physics and Chemistry, University of Palermo, Via Archirafi, 36, 90123 Palermo, Italy

* Correspondence: monia.spera@imm.cnr.it (M.S.); giuseppe.greco@imm.cnr.it (G.G.)

Received: 16 May 2019; Accepted: 3 July 2019; Published: 10 July 2019

Abstract: This paper compares the metal/semiconductor barrier height properties of non-recessed Ti/Al/Ti and Ta/Al/Ta contacts on AlGaN/GaN heterostructures. Both contacts exhibited a rectifying behavior after deposition and after annealing at temperatures up to 550 °C. The ohmic behavior was reached after annealing at 600 °C. High-resolution morphological and electrical mapping by conductive atomic force microscopy showed a flat surface for both contacts, with the presence of isolated hillocks, which had no significant impact on the contact resistance. Structural analyses indicated the formation of the Al_3Ti and Al_3Ta phases upon annealing. Furthermore, a thin interfacial TiN layer was observed in the Ti/Al/Ti samples, which is likely responsible for a lower barrier and a better specific contact resistance ($\rho_c = 1.6 \times 10^{-4}$ Ωcm^2) with respect to the Ta/Al/Ta samples ($\rho_c = 4.0 \times 10^{-4}$ Ωcm^2). The temperature dependence of the specific contact resistance was described by a thermionic field emission mechanism, determining barrier height values in the range of 0.58–0.63 eV. These results were discussed in terms of the different microstructures of the interfaces in the two systems.

Keywords: AlGaN/GaN; ohmic contacts; barrier height; Ti/Al/Ti; Ta/Al/Ta

---

1. Introduction

Gallium Nitride (GaN) and relative alloys have been considered as very good materials for modern high-power and high-frequency devices to replace existing silicon (Si) technology [1,2]. In particular, the existence of a two-dimensional electron gas (2DEG) in AlGaN/GaN heterostructures is the key feature for the fabrication of high electron mobility transistors (HEMTs) [3]. For these devices, a low resistance of the source and drain ohmic contacts is mandatory to reduce the total device on-resistance.

The formation mechanisms of ohmic contacts on AlGaN/GaN heterostructures have been widely studied in recent decades [4]. Generally, Ti/Al/γ/Au metal multilayers (where γ = Ni, Mo, Ti . . .) can be used to achieve an ohmic behavior upon annealing at 800–850 °C [4–6], in which the single layers play a specific role. Specifically, the uppermost Au layer is aimed at preventing surface oxidation [7], but it also forms highly conductive phases upon annealing, which improve the overall electrical conduction of the reacted stack and its contact resistance [8]. At the same time, however, the presence of Au induces a high surface roughness in the reacted contacts [8,9] and, hence, a poor edge acuity of the lithographically defined electrodes that can be detrimental for the final device reliability.

Recently, GaN-on-Si epitaxial wafers up to 200 mm in diameter, of adequate electronic quality, for HEMT fabrication have been demonstrated [10]. Hence, the possibility to integrate GaN HEMT

technology on the existing Si Complementary Metal-Oxide Semiconductor (CMOS) platforms opened a series of manufacturing challenges [11]. As an example, in order to have GaN devices processing to be adaptable to a Si CMOS environment, the traditional Ti/Al/γ/Au schemes must be replaced by "Au-free" ohmic contacts.

The easiest approach to fabricate ohmic contacts without gold ("Au-free"), is to remove the uppermost Au layer in the stack. In particular, to this aim, many authors proposed the use of low work-function Ti-based or Ta-based systems (Ti/Al, Ta/Al, Ti/Al/TiN) [12–18], to obtain a low Schottky barrier height Φ_B with AlGaN and, hence, a low value of specific contact resistance ρ_c [Ωcm^2]. All these works revealed the importance of several parameters, such as the thermal annealing processes, the metal's thickness or the GaN material quality [15,16,19,20].

In this context, although many papers have reported on Ti- or Ta- based ohmic contact [4,13,14,16,18,19,21], these systems deserve further investigations for a better comprehension of their electrical behavior. Indeed, in the literature, there is a lack of information on the barrier height properties and on the carrier transport mechanisms at these interfaces.

In this study, the electrical, structural and morphological properties of Ti/Al/Ti and Ta/Al/Ta contacts on AlGaN/GaN heterostructures have been monitored as a function of the annealing temperature. The temperature behavior of the specific contact resistance $\rho_c(T)$ enabled us to identify the dominant transport mechanism at the metal/AlGaN interface and to determine the barrier height values in the two systems. The electrical results have been linked to the structural and morphological modifications occurring after the annealing process.

2. Materials and Methods

Our experiments were performed on $Al_{0.26}Ga_{0.74}N$/GaN heterostructures grown onto Si wafers. The AlGaN barrier layer was 16 nm thick, while the two dimensional electron gas (2DEG) exhibited a sheet carrier density of 7.45×10^{12} cm^{-2}. First, the sample's surface was subjected to a cleaning process in diluted HF:HCl solution. Two Ti- and Ta-based metal stacks deposited by sputtering were compared, i.e., $Ti_{(10nm)}/Al_{(300nm)}/Ti_{(20nm)}$ and $Ta_{(10nm)}/Al_{(300nm)}/Ta_{(20nm)}$. For the electrical characterization, linear Transmission Line Model (TLM) structures were defined by optical lithography and lift-off. The TLM geometry consisted of rectangular pads (100 µm × 200 µm), at distances d varying between 20 and 100 µm. The lateral isolation of the TLM patterns was obtained by a plasma etch. Then, rapid thermal annealing (RTA) processes of the samples were performed in Ar atmosphere in the temperature range 400–600 °C, using a Jipelec JetFirst 150 furnace. The electrical properties of the contacts were monitored after each annealing step, and the specific contact resistance ρ_c was determined using the standard TLM method [22]. The current–voltage (I–V) measurements on the TLM structures were performed on a Karl Suss Microtec probe station equipped with a HP 4156B parameter analyzer, in a four-point probe configuration. X-ray diffraction (XRD) was used in order to monitor the microstructure of the annealed contacts. The measurements were performed in grazing mode, using a Bruker-AXS D5005 θ-θ diffractometer operating with a Cu Ka radiation at 40 kV and 30 mA. A correlation between the surface morphological properties and the local electrical response of the material was made by Atomic Force Microscopy (AFM) and Conductive Atomic Force Microscopy (C-AFM), using a Veeco Dimension 3100 microscope with a Nanoscope V controller. A 200 kV JEOL 2010 F microscope was used to perform cross-sectional Transmission Electron Microscopy (TEM) analyses of the samples and to look at the metal/semiconductor interface.

3. Results

The I–V characteristics of the contacts showed a non-linear behavior after deposition. Figure 1 shows the I–V curves acquired on Ta/Al/Ta (Figure 1a) and Ti/Al/Ti (Figure 1b) TLM structures at different annealing temperatures. The curves are measured between contact pads placed at a distance of 20 µm. As can be seen, both contacts exhibit a rectifying behavior after deposition and after annealing at temperatures up to 550 °C. The ohmic behavior is reached after annealing at 600 °C.

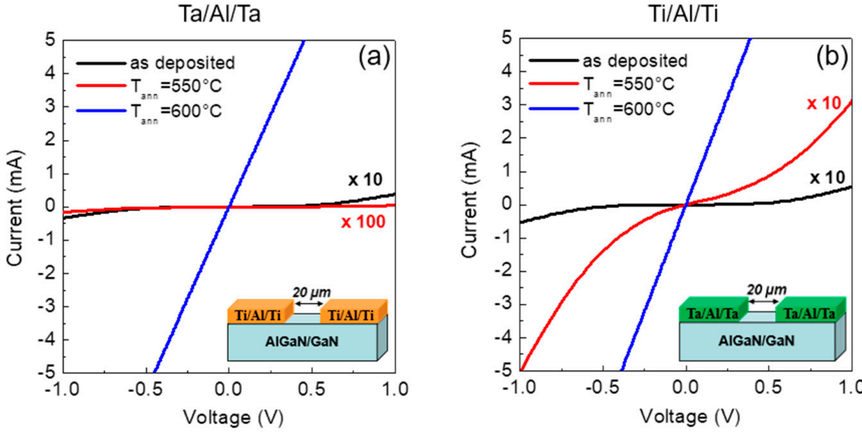

Figure 1. Current–voltage (I–V) curves acquired on pads of Transmission Line Model (TLM) structures at a distance of 20 μm in (**a**) Ta/Al/Ta and (**b**) Ti/Al/Ti treated at different annealing temperatures (as deposited, 550 °C and 600 °C).

While in the case of Ti-based contact an annealing process of 60 s at 600 °C already leads to ohmic behavior, a longer annealing duration (180 s) was needed for the Ta-based contact. Then, for our study we selected the contacts at the onset of their ohmic behavior, i.e., the Ta/Al/Ta contacts annealed at 600 °C for 180 s and the Ti/Al/Ti contacts annealed at 600 °C for 60 s.

The I–V curves acquired on TLM structures in both Ta/Al/Ta (600 °C, 180 s) and Ti/Al/Ti (600 °C, 60 s) are shown in Figure 2a,b, respectively. As can be seen, linear characteristics are observed in both cases, with the current decreases with increasing TLM pad distance. Moreover, Ti/Al/Ti contacts show a higher current level. From the slope of these curves, it was possible to extract the total resistance R_{TOT}. In particular, Figure 2c reports the plot of the total resistance R_{TOT} measured as a function of the distance d between adjacent TLM pads, showing a linear increase in the resistance.

From the analysis of several TLM patterns, similar values of sheet resistance R_{SH} were extracted for the two samples, i.e., R_{SH} = 472 ± 10 Ω/□ for the Ti/Al/Ti sample and R_{SH} = 475 ± 9 Ω/□ for the Ta/Al/Ta sample. The value of the specific contact resistance ρ_c extracted for the Ti/Al/Ti contacts was $\rho_{c(Ti/Al/Ti)} = 1.6 \pm 0.6 \times 10^{-4}$ Ωcm^2, i.e., more than a factor of two lower than the value extracted in Ta/Al/Ta ($\rho_{c\ (Ta/Al/Ta)} = 4.0 \pm 1.1 \times 10^{-4}$ Ωcm^2).

In order to explain these differences and to understand the mechanism of ohmic contact formation in the two systems, a morphological and structural characterization of the samples was carried out. Figure 3a,b show the morphologies of the Ti/Al/Ti and Ta/Al/Ta contacts annealed at 600 °C, acquired on a 40 μm × 40 μm region. In both cases, the surface is characterized by flat areas with some isolated hillocks, leading to root mean square (RMS) roughness values of 48 nm and 79 nm for Ta- and Ti-based contacts, respectively. These hillocks are more pronounced in the case of the Ti/Al/Ti system, thus justifying the higher RMS value. Figure 3c,d show the AFM images acquired on the flat areas on a 5 μm × 5 μm region. Interestingly, also in the flatter areas the Ta/Al/Ta contacts exhibited a lower roughness (RMS = 14.2 nm) with respect to the Ti/Al/Ti samples (RMS = 18.5 nm).

It is noteworthy that, besides the contribution of the isolated hillocks, the two Au-free systems exhibited a flatter surface compared with that of the standard Ti/Al/Ni/Au contacts, which showed an ohmic behavior at 800 °C [23], thus representing a major advantage for device fabrication, from a technological point of view. However, the nature of these hillocks must be further investigated in order to pave the route to avoid their formation and to further optimize the morphology of the contacts.

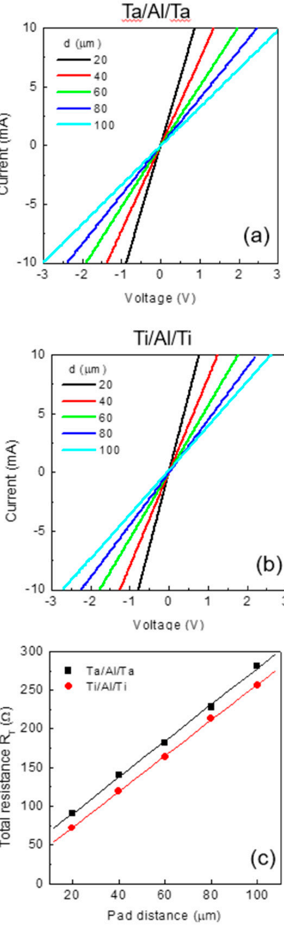

Figure 2. I–V curves acquired on TLM structures in (**a**) Ta/Al/Ta and (**b**) Ti/Al/Ti contacts annealed at 600 °C. (**c**) Characteristic plot of the total resistance R_{TOT} measured as a function of the adjacent TLM pads' distance *d* for Ta/Al/Ta (squares) and Ti/Al/Ti (circles).

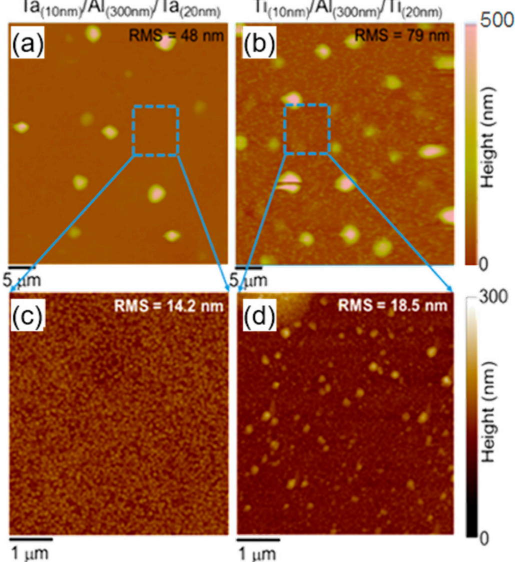

Figure 3. Atomic Force Microscopy (AFM) images of contacts on AlGaN/GaN heterostructure: (**a**) AFM images of Ta/Al/Ta contact on 40 µm × 40 µm and (**b**) 5 µm × 5 µm scan areas, and (**c**) AFM images of Ti/Al/Ti contact on 40 µm × 40 µm and (**d**) 5 µm × 5 µm scan areas, after annealing at 600 °C.

To electrically characterize the nature of these hillocks, the surface morphology and local current maps were acquired on the Ti/Al/Ti and Ta/Al/Ta samples by C-AFM. During surface scanning with a conductive diamond-coated tip, a positive bias of +5 V was applied to the samples' backside, and the current flowing to the tip across the metal/semiconductors interface was collected by a current amplifier connected to the tip. A representative morphological image and the corresponding current map on a 20 µm × 20 µm scan area for the Ta/Al/Ta sample are shown in Figure 4a,b, respectively. The morphological and electrical analyses performed under the same conditions on the Ti/Al/Ti sample are reported in Figure 4c,d. A clear correlation between the surface features and the current maps is visible on both samples. In particular, a uniform current level is detected in the flat areas of the samples. Furthermore, the hillocks in the Ta-based contacts display a higher conductivity with respect to the uniform background of the surrounding metal surface, whereas a lower conductivity has been observed over the hillocks in the Ti-based contacts. The different composition (e.g., the phase or the Al content present in the core of the hillocks) can be responsible for the different conductivity detected by C-AFM analyses. However, the area occupied by the hillocks is only ~1% and ~5% of the overall contact area in Ta- and Ti-based systems, respectively. Hence, the contribution to the increase or the decrease in the total current flowing across the overall contact area is in the order of 1–2% in both cases. Then, we can conclude that the presence of these hillocks on the surface does not significantly impact the specific contact resistance.

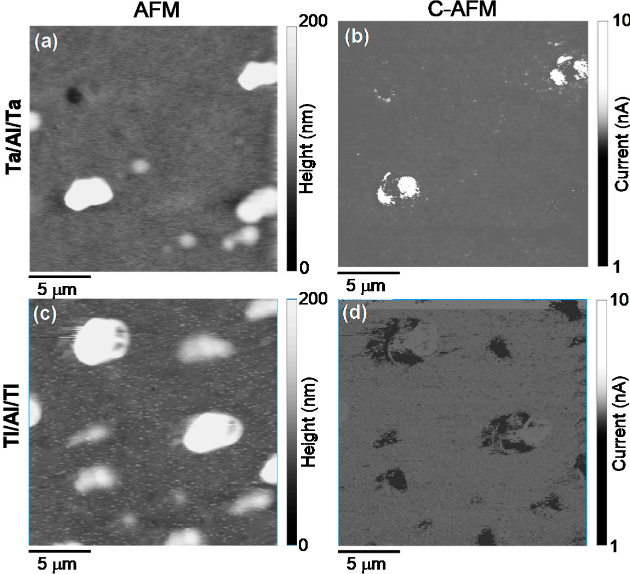

Figure 4. AFM image and Conductive Atomic Force Microscopy (C-AFM) map acquired on contacts: (**a**) AFM image and (**b**) associated C-AFM map acquired on Ta/Al/Ta contact. (**c**) AFM image and (**d**) associated C-AFM map acquired on Ti/Al/Ti contact. The images were acquired on 20 µm × 20 µm scan areas.

XRD analysis, shown in Figure 5, was carried out to identify the phases formed in the layer after the annealing process at 600 °C. The XRD patterns of the Ti/Al/Ti contact are associated to the presence of the Al_3Ti phase and unreacted Al. Indeed, for annealing temperatures higher than 450 °C, Ti typically reacts with Al and forms the Al_3Ti phase [16,24]. However, the segregation of unreacted Al from the Al_3Ti phase can occur at higher annealing temperatures [14], which is consistent with our experimental observation. An analogous behavior has been observed in the annealed Ta/Al/Ta contact, where the Al_3Ta was the main phase detected by XRD, with unreacted Al still present in the system. In fact, the formation of the Al_3Ta phase is expected in a temperature range between 600 and 1500 °C [14,16]. For the annealing temperature considered in our case, Al_3Ta and Al_3Ti are the most thermodynamically favored phases [25].

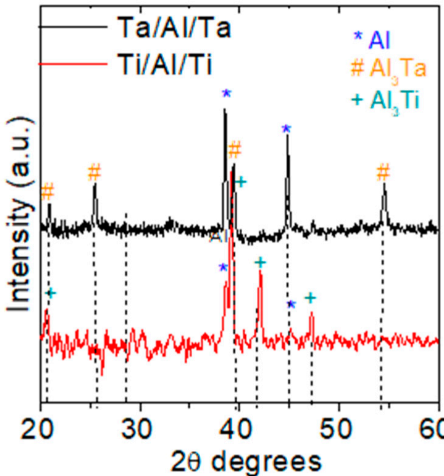

Figure 5. X-ray diffraction (XRD) patterns for Ta/Al/Ta and Ti/Al/Ti contacts annealed at 600 °C, showing the appearance of the Al_3Ta and Al_3Ti phases.

An analytical description of the carrier's transport mechanism through the metal/semiconductor interfaces was obtained by monitoring the temperature dependence of the electrical parameters. For this purpose, the TLM measurements were performed at temperatures between 25 °C and 175 °C, and the R_{SH} and ρ_c values were determined at each measurement temperature T.

Figure 6 shows the values of R_{SH} of the two samples as a function of the measurement temperature T. As can be seen, the values of R_{SH} are very similar in both cases and increase with the temperature. The sheet resistance R_{SH} depends on the 2DEG density n_s and on mobility μ following the expression

$$R_{SH} = \frac{1}{q n_s \mu} \tag{1}$$

In our case, according to Hall measurements, the 2DEG density n_s did not show significant variations with temperature, as commonly reported in literature for AlGaN/GaN heterostructures [26]. Hence, the temperature dependence of R_{SH} is mostly related to the carrier mobility. Accordingly, R_{SH} could be fitted using a power-law expression, like $R_{SH} \propto T^{\beta}$, typically used for the temperature dependence of 2DEG mobility ($\mu \propto T^{-\beta}$) [27,28]. The fit of the experimental data, reported as a continuous line in Figure 6, returned a value of $\beta = 2.87$, which is consistent with the dominance of the optical phonon scattering mechanism [6,26].

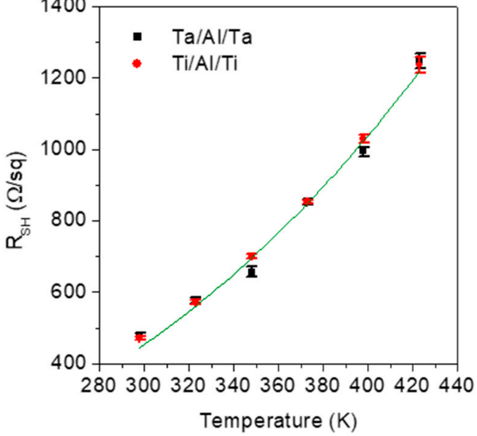

Figure 6. Sheet resistance R_{SH} versus temperature T for the AlGaN/GaN heterostructures with Ta/Al/Ta (squares) and Ti/Al/Ti (circles) contacts. The continuous lines represent the fits of the experimental data obtained assuming $R_{SH} \propto T^{\beta}$, with $\beta = 2.87$.

Figure 7 reports the values of ρ_c versus the measurement temperature T for the two contacts. Evidently, a similar trend of the $\rho_c(T)$ is noticed in both samples. The measured values of ρ_c become lower by increasing the measurement temperature T.

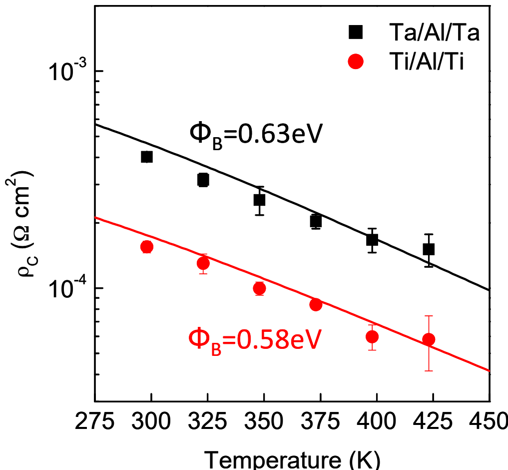

Figure 7. Temperature dependence of specific contact resistance ρ_C for the Ta/Al/Ta (squares) and Ti/Al/Ti (circles) contacts annealed at 600 °C. The lines represent the fits of the experimental data with the thermionic field emission (TFE) model (Equation (2)).

The experimental values of ρ_c were well fitted by the thermionic field emission (TFE) mechanism, using the following expression [29]:

$$\rho_C = \left(\frac{1}{qA^*}\right)\frac{k^2}{\sqrt{\pi(\Phi_B + V_n)E_{00}}}\cosh\left(\frac{E_{00}}{kT}\right)\sqrt{\coth\left(\frac{E_{00}}{kT}\right)}\exp\left(\frac{\Phi_B + V_n}{E_0} - \frac{V_n}{kT}\right) \quad (2)$$

where

$$E_0 = E_{00}\coth\left(\frac{E_{00}}{kT}\right) \quad (3)$$

and A^* is the Richardson constant, V_n is the distance of the Fermi level from the conduction band minimum, k is the Boltzmann constant, T is the absolute temperature and E_{00} is the characteristic energy described by

$$E_{00} = \frac{qh}{4\pi}\sqrt{\left(\frac{N_D}{m^*\varepsilon}\right)} \quad (4)$$

where h is the Planck constant, N_D is the carrier concentration, m^* is the tunneling effective mass and ε is the dielectric constant of the AlGaN.

The values of the Schottky barrier height extrapolated from the fit of the experimental data were Φ_B = 0.58 eV for Ti/Al/Ti and Φ_B = 0.63 eV for Ta/Al/Ta, with a carrier concentration of $N_D = 1.25 \times 10^{19}$ cm^{-3} for both contacts. This high value of N_D determined from the fit is consistent with the presence of 2DEG. For that reason, in the following this value will be regarded as N_{D_2DEG}.

In the case of AlGaN/GaN heterostructures, the presence of 2DEG influences the mechanism of current transport at the interface [27,30]. Many literature works used the TFE model to describe the current transport in annealed ohmic contacts on AlGaN/GaN heterostructures [6,27,31,32]. In this case, the carrier concentration N_{D_2DEG} can be expressed as a function of the 2DEG sheet carrier density n_s and of the AlGaN thickness d_{AlGaN} [33]:

$$N_{D_2DEG} = \frac{n_s(d_{AlGaN})}{d_{AlGaN}} \quad (5)$$

However, the 2DEG carrier density depends on the AlGaN/GaN heterostructure's properties [34]. In particular, the 2DEG carrier density decreases with decreasing d_{AlGaN}, until it is completely depleted for values lower than a critical thickness [35]. This behavior strongly influences the characteristic energy E_{00}, which depends on N_{D_2DEG} in AlGaN/GaN heterostructures, and then ultimately on the d_{AlGaN}. Hence, the transparency of the barrier will be expressed by:

$$E_{00_2DEG} = \frac{qh}{4\pi}\sqrt{\frac{n_s(d_{AlGaN})}{d_{AlGaN}\ m^*\ \varepsilon}} \tag{6}$$

Similarly to the classical TFE mechanism, where ρ_c depends on the Schottky barrier height and on the characteristic energy, in the presence of 2DEG the proportionality between the specific contact resistance ($\rho_{cC(TFE\text{-}2DEG)}$) and Φ_B and E_{00_2DEG} will become:

$$\rho_{C(TFE-2DEG)} \propto exp\left(\frac{\Phi_B}{E_{00_2DEG}(d_{AlGaN})coth\left(\frac{E_{00_2DEG}(d_{AlGaN})}{kT}\right)}\right) \tag{7}$$

Figure 8 reports the specific contact resistance ρ_c versus the AlGaN thickness (d_{AlGaN}) for Ta/Al/Ta and Ti/Al/Ti ohmic contacts on AlGaN/GaN heterostructures, calculated using the TFE-2DEG model.

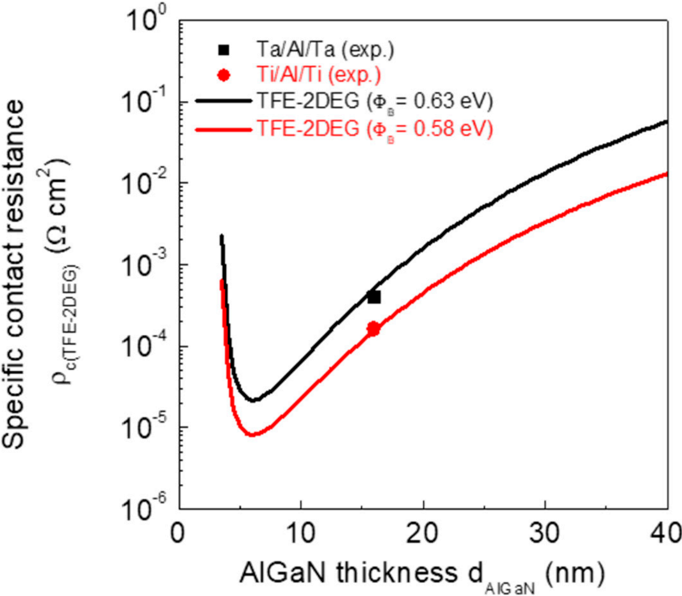

Figure 8. Specific contact resistance $\rho_{C(TFE\text{-}2DEG)}$ versus the AlGaN thickness (d_{AlGaN}) for Ta/Al/Ta and Ti/Al/Ti Ohmic contacts on AlGaN/GaN heterostructures, calculated using the TFE-2DEG model (Al concentration of 26%). The experimental data points are also reported.

An AlGaN/GaN heterostructure with an Al concentration of 26% was considered in this calculation. The values Φ_B = 0.63 eV and Φ_B = 0.58 eV were used to calculate the specific contact resistance in annealed Ta/Al/Ta and Ti/Al/Ti contacts, respectively. As can be seen, the experimental values of ρ_c are in agreement with those predicted by the model. The calculated ρ_c curves suggest that a further lowering of the specific contact resistance could be obtained by a reduction of the AlGaN barrier layer thickness d_{AlGaN} down to 5–10 nm. However, an additional reduction of d_{AlGaN} leads to a further depletion of the 2DEG, which results in a decrease in E_{00_2DEG}. This behavior ultimately results in an increase in $\rho_{c(TFE\text{-}2DEG)}$ for a very thin AlGaN barrier layer. To further explain the different electrical properties of the interfaces in the annealed Ti/Al/Ti and Ta/Al/Ta stacks, a structural inspection of the reacted layers was carried out by means of cross-sectional TEM analyses together with high angle

annular dark field (HAADF) acquisition in scanning mode, more sensitive to heavy atoms. Figure 9 shows TEM (Figure 9a,b) and Scanning Transmission Electron Microscopy (STEM) (Figure 9c,d) pictures of the two samples after the annealing at 600 °C.

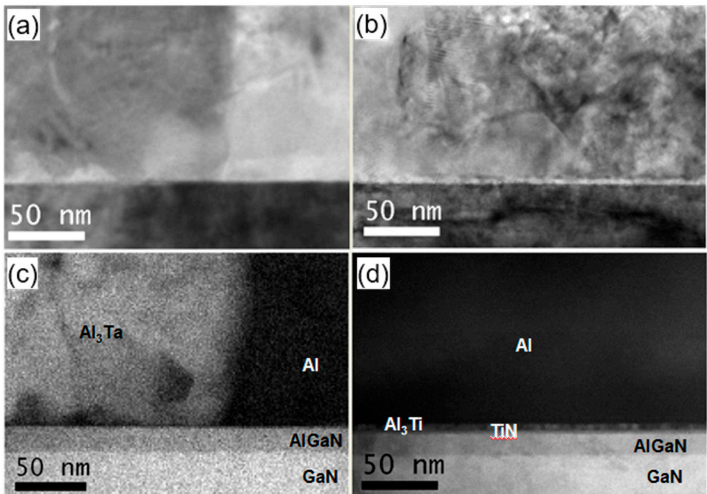

Figure 9. Cross-section Transmission Electron Microscopy (TEM) images of Ta/Al/Ta (**a**) and Ti/Al/Ti (**b**) contacts, and Scanning Transmission Electron Microscopy (STEM) images of Ta/Al/Ta (**c**) and Ti/Al/Ti (**d**) annealed at 600 °C.

Clearly, the annealing treatment induced an interaction of the metal layers and a modification of the interfacial region close to the AlGaN. In fact, two different interface structures were observed. In the Ti/Al/Ti contact, the titanium atoms are mainly detected at the interface, in the form of a continuous TiN layer of a few nanometers with a mixed Al-Ti layer above it. The rest of the film is composed of pure Al (Figure 9b,d). In the Ta/Al/Ta system, all the tantalum atoms reacted with Al, generating large Al_3Ta grains coexisting with pure unreacted Al. These Al_3Ta grains are often very large, entirely covering a region from the AlGaN/GaN interface to the contact surface (see Figure 9a,c). However, low-resolution TEM images (not reported) showed that the Al_3Ta grains are still covered by a Ta layer at the sample surface.

Many works in literature [36–39] described the reaction between Ti and GaN (or AlGaN), leading to TiN formation at the interface. In bulk material, the release of nitrogen vacancies acting as donors typically raises the net carrier concentration below the metal close to the interface [9,40]. However, while the temperature dependence of ρ_c in n-type doped (~ 10^{18} cm^{-3}) bulk materials can reveal an increase in the carrier concentration [9], this is much more difficult in the presence of 2DEG, i.e., where a higher density of carriers (~10^{19}–10^{20} cm^{-3}) is already present close to the interface [6,27,30,41]. On the other hand, TiN formation can be a key factor for the reduction of the barrier height in annealed Ti/Al/Ti ohmic contacts.

Such a kind of structural interaction of the metal with the substrate was not observed in the case of Ta-based contacts, which in fact required a longer annealing time to reach the ohmic behavior and exhibited a higher ρ_c. The ease of reaction of Ti with respect to Ta can be explained by the larger negative heat of the formation of TiN (−336 kJ/mol) with respect to TaN (−247 kJ/mol) [7]. Hence, it can be argued that the different interfacial microstructures are responsible for the different values of Φ_B extrapolated from the temperature dependence of ρ_c.

4. Conclusions

In summary, the morphological, structural and electrical properties of non-recessed Ti- and Ta-based contacts were comparatively investigated. Both contacts show an ohmic behavior after an annealing temperature of 600 °C, with specific contact resistance values of 1.6×10^{-4} Ωcm^2 for

Ti/Al/Ti contacts and 4.0×10^{-4} Ωcm^2 for Ta/Al/Ta contacts. The temperature dependence of $\rho_c(T)$ was explained by the TFE mechanism, determining Schottky barrier height values of 0.58 eV for Ti/Al/Ti and 0.63 eV for Ta/Al/Ta. These results were correlated to the different microstructures of the reacted stacks. In particular, the creation of a TiN layer at the interface in the Ti/Al/Ti sample is likely the key factor for the lower barrier height and better specific contact resistance. Both samples showed a flat surface morphology after annealing, besides some isolated hillocks which had no significant impact on the overall contact resistance. However, as the presence of these morphological features can be detrimental for a device's reliability, further work is still required to optimize the contact composition and to obtain a further improvement of the contact surface.

Beyond their fundamental importance from a materials science point of view, these results can have also relevant implications for GaN-on-Si device technology.

Author Contributions: The authors contributed to this work as follows: electrical measurements and manuscript writing M.S., G.G.; structural analyses R.L.N., S.S., C.B.; C-AFM analyses and manuscript writing F.G.; supervision M.C.; scientific coordination, manuscript writing and review F.R.

Funding: This work was carried out within the National Project PON EleGaNTe (Electronics on GaN-based Technologies), ARS01_01007, funded by the Italian Ministry for Education, University and Research (MIUR).

Acknowledgments: The authors would like to thank S. Di Franco (CNR-IMM) for his technical support during clean room sample processing. Moreover, F. Iucolano (STMicroelectronics) and his team are recognized for the productive discussions on the results and support during the electrical characterization.

Conflicts of Interest: The authors declare no conflict of interest.

References

1. Meneghini, M.; Meneghesso, G.; Zanoni, E. *Power GaN Devices Materials, Applications and Reliability*; Springer International Publishing: Basel, Switzerland, 2017.
2. Roccaforte, F.; Fiorenza, P.; Greco, G.; Nigro, R.L.; Giannazzo, F.; Iucolano, F.; Saggio, M. Emerging trends in wide band gap semiconductors (SiC and GaN) technology for power devices. *Microelectron. Eng.* **2018**, *187–188*, 66–77. [CrossRef]
3. Roccaforte, F.; Fiorenza, P.; Nigro, R.L.; Giannazzo, F.; Riv, G.G. Physics and technology of gallium nitride materials for power electronics. *Nuovo Cimento* **2018**, *41*, 625–681.
4. Greco, G.; Iucolano, F.; Roccaforte, F. Ohmic contacts to Gallium Nitride materials. *Appl. Surf. Sci.* **2016**, *383*, 324. [CrossRef]
5. Wang, L.; Mohammed, F.M.; Adesida, I. Differences in the reaction kinetics and contact formation mechanisms of annealed Ti/Al/Mo/Au Ohmic contacts on n-GaN and AlGaN/GaN epilayers. *Appl. Phys.* **2007**, *101*, 013702. [CrossRef]
6. Iucolano, F.; Greco, G.; Roccaforte, F. Correlation between microstructure and temperature dependent electrical behavior of annealed Ti/Al/Ni/Au Ohmic contacts to AlGaN/GaN heterostructures. *Appl. Phys. Lett.* **2013**, *103*, 201604. [CrossRef]
7. Mohammad, S.N. Contact mechanisms and design principles for alloyed ohmic contacts to n-GaN. *J. Appl. Phys.* **2004**, *95*, 7940. [CrossRef]
8. Roccaforte, F.; Iucolano, F.; Giannazzo, F.; Alberti, A.; Raineri, V. Nanoscale carrier transport in Ti/Al/Ni/Au Ohmic contacts on AlGaN epilayers grown on Si(111). *Appl. Phys. Lett.* **2006**, *89*, 022103. [CrossRef]
9. Iucolano, F.; Roccaforte, F.; Alberti, A.; Bongiorno, C.; di Franco, S.; Raineri, V. Temperature dependence of the specific resistance in Ti/Al/Ni/Au contacts on n-type GaN. *J. Appl. Phys.* **2006**, *100*, 123706. [CrossRef]
10. Tripathy, S.; Lin, V.K.X.; Dolmanan, S.B.; Tan, J.P.Y.; Kajen, R.S.; Bera, L.K.; Teo, S.L.; Kumar, M.K.; Arulkuumanaran, S.; Ng, G.I.; et al. AlGaN/GaN two-dimensional-electron gas heterostructures on 200 mm diameter Si(111). *Appl. Phys. Lett.* **2012**, *101*, 082110. [CrossRef]
11. Marcon, D.; de Jaeger, B.; Halder, S.; Vranckx, N.; Mannaert, G.; van Hove, M.; Decoutere, S. Manufacturing Challenges of GaN-on-Si HEMTs in a 200 mm CMOS Fab. *IEEE Trans. Semicond. Manufact.* **2013**, *26*, 361. [CrossRef]
12. Liu, X.; Zhan, C.; Chan, K.W.; Liu, W.; Tan, L.S.; Chen, K.J.; Yeo, Y.C. AlGaN/GaN-on-Silicon Metal–Oxide–Semiconductor High-Electron-Mobility Transistor with Breakdown Voltage of 800 V and

On-State Resistance of 3 mΩcm2 Using a Complementary Metal–Oxide–Semiconductor Compatible Gold-Free Process. *Appl. Phys. Express* **2012**, *5*, 066501. [CrossRef]
13. Malmros, A.; Blanck, H.; Rorsman, N. Electrical properties, microstructure, and thermal stability of Ta-based ohmic contacts annealed at low temperature for GaN HEMTs. *Semicond. Sci. Technol.* **2011**, *26*, 075006. [CrossRef]
14. Costant, A.; Baele, J.; Coppens, P.; Qin, W.; Ziad, H.; de Backer, E.; Moens, P.; Tack, M. Impact of Ti/Al atomic ratio on the formation mechanism of non-recessed Au-free Ohmic contacts on AlGaN/GaN heterostructures. *J. Appl. Phys.* **2016**, *120*, 104502. [CrossRef]
15. Pooth, A.; Bergsten, J.; Rorsman, N.; Hirshy, H.; Perks, R.; Tasker, P.; Martin, T.; Webster, R.F.; Cherns, D.; Uren, M.J.; et al. Morphological and electrical comparison of Ti and Ta based ohmic contacts for AlGaN/GaN-on-SiC HFETs. *Microelectron. Reliab.* **2017**, *68*, 2–4. [CrossRef]
16. Greco, G.; Giannazzo, G.; Iucolano, F.; Nigro, R.L.; Roccaforte, F. Nanoscale structural and electrical evolution of Ta-and Ti-based contacts on AlGaN/GaN heterostructures. *J. Appl. Phys.* **2013**, *114*, 083717. [CrossRef]
17. Van Daele, B.; van Tendeloo, G.; Ruythooren, W.; Derluyn, J.; Leys, M.R.; Germain, M. The role of Al on Ohmic contact formation on n-type GaN and AlGaN/GaN. *Appl. Phys. Lett.* **2005**, *87*, 061905. [CrossRef]
18. Firrincielli, A.; de Jaeger, B.; You, S.; Wellekens, D.; van Hove, M.; Decoutere, S. Au-free low temperature ohmic contacts for AlGaN/GaN power devices on 200 mm Si substrates. *Jpn. J. Appl. Phys.* **2014**, *53*, 04EF01. [CrossRef]
19. Greco, G.; Iucolano, F.; Bongiorno, C.; Giannazzo, F.; Krysko, M.; Leszczynski, M.; Roccaforte, F. Ti/Al ohmic contacts on AlGaN/GaN heterostructures with different defect density. *Appl. Surf. Sci.* **2014**, *314*, 546–551. [CrossRef]
20. Greco, G.; Iucolano, F.; Bongiorno, C.; di Franco, S.; Nigro, R.L.; Giannazzo, F.; Prystawko, P.; Kruszewski, P.; Krysko, M.; Grzanka, E.; et al. Electrical and structural properties of Ti/Al-based contacts on AlGaN/GaN heterostructures with different quality. *Phys. Status Solidi* **2015**, *212*, 1091–1098. [CrossRef]
21. E-Zammar, G.; Yvon, A.; Khalfaoui, W.; Nafouti, M.; Cayrel, F.; Collard, E.; Alquier, D. A simple non-recessed and Au-free high quality Ohmic contacts on AlGaN/GaN: The case of Ti/Al alloy. *Mater. Sci. Semicond. Proc.* **2018**, *78*, 107–110. [CrossRef]
22. Berger, H.H. Models for contacts to planar devices. *Solid State Electron.* **1972**, *15*, 145–158. [CrossRef]
23. Spera, M.; Miccoli, C.; Nigro, R.L.; Bongiorno, C.; Corso, D.; di Franco, S.; Iucolano, F.; Roccaforte, F.; Mater, G.G. Modification of the sheet resistance under Ti/Al/Ni/Au Ohmic contacts on AlGaN/GaN heterostructures. *Sci. Semicond. Process.* **2018**, *78*, 111. [CrossRef]
24. Sujata, M.; Bhargava, S.; Sangal, S. On the formation of TiAl3 during reaction between solid Ti and liquid Al. *J. Mater. Sci. Lett.* **1997**, *16*, 1175. [CrossRef]
25. Pretorius, R.; Vredenberg, A.M.; Saris, F.W.; de Reus, R. Silicide formation by concentration controlled phase selection. *J. Appl. Phys.* **1991**, *70*, 3636. [CrossRef]
26. Hofman, T.; Kühne, P.; Schöche, S.; Chen, J.T.; Forsberg, U.; Janzén, E.; Sedrine, N.B.; Herzinger, C.M.; Woollam, J.A.; Schubert, M.; et al. Temperature dependent effective mass in AlGaN/GaN high electron mobility transistor structures. *Appl. Phys. Lett.* **2012**, *101*, 192102. [CrossRef]
27. Liu, Z.H.; Arulkumaran, S.; Ng, G.I. Temperature dependence of Ohmic contact characteristics in AlGaN/GaN high electron mobility transistors from −50 to 200 °C. *Appl. Phys. Lett.* **2009**, *94*, 142105. [CrossRef]
28. Gaska, R.; Yang, J.W.; Osinsky, A.; Chen, Q.; Khan, M.A.; Orlov, A.O.; Snider, G.L.; Shur, M.S. Electron mobility in modulation-doped AlGaN–GaN heterostructures. *Appl. Phys. Lett.* **1998**, *72*, 707. [CrossRef]
29. Padovani, F.A.; Stratton, R. Field and thermionic-field emission in Schottky barriers. *Solid-State Electron.* **1966**, *9*, 695. [CrossRef]
30. Takei, Y.; Kamiya, M.; Tsutsui, K.; Saito, W.; Kakushima, K.; Wakabayashi, H.; Kataoka, Y.; Iwai, H. Ohmic Contact Properties Depending on AlGaN Layer Thickness for AlGaN/GaN High Electron Mobility Transistor Structures. *ECS Trans.* **2014**, *61*, 265. [CrossRef]
31. Yoshida, T.; Egawa, T. Dynamic variation of carrier transport properties of recessed Au-free ohmic contacts to InAlN/AlN/GaN on Si-wafer. *Jpn. J. Appl. Phys.* **2018**, *57*, 110302.
32. Liu, Y.; Singh, S.P.; Kyaw, L.M.; Bera, M.K.; Ngoo, Y.J.; Tan, H.R.; Tripathy, S.; Lo, G.Q.; Chor, E.F. A Mechanisms of ohmic contact formation and carrier transport of low temperature annealed Hf/Al/Ta on In 0.18 Al 0.82 N/GaN-on-Si. *ECS J. Solid. State Sci. Technol.* **2015**, *4*, 30. [CrossRef]

33. Nam, T.C.; Jang, J.S.; Seong, T.Y. Carrier transport mechanism of strained AlGaN/GaN Schottky contacts. *Cur. Appl. Phys.* **2012**, *12*, 1081. [CrossRef]
34. Ambacher, O.; Smart, J.; Shealy, J.R.; Weimann, N.G.; Chu, K.; Murphy, M.; Schaff, W.J.; Eastman, L.F.; Dimitrov, R.; Wittmer, L.; et al. Two-dimensional electron gases induced by spontaneous and piezoelectric polarization charges in N- and Ga-face AlGaN/GaN heterostructures. *J. Appl. Phys.* **1999**, *85*, 3222. [CrossRef]
35. Ibbetson, J.P.; Fini, P.T.; Ness, K.D.; DenBaars, S.P.; Speck, J.S.; Mishra, U.K. Polarization effects, surface states, and the source of electrons in AlGaN/GaN heterostructure field effect transistors. *Appl. Phys. Lett.* **2000**, *77*, 250. [CrossRef]
36. Lin, Y.J.; Chen, Y.M.; Cheng, T.J.; Ker, Q. Schottky barrier height and nitrogen–vacancy-related defects in Ti alloyed Ohmic contacts to n-GaN. *J. Appl. Phys.* **2004**, *95*, 571. [CrossRef]
37. Luther, B.P.; Mohney, S.E.; Jackson, T.N.; Khan, M.A.; Chen, Q.; Yang, J.W. Investigation of the mechanism for Ohmic contact formation in Al and Ti/Al contacts to n-type GaN. *Appl. Phys. Lett.* **1997**, *70*, 57. [CrossRef]
38. Motayed, A.; Bathe, R.; Wood, M.C.; Diouf, O.S.; Vispute, R.D.; Mohammad, S.N. Electrical, thermal, and microstructural characteristics of Ti/Al/Ti/Au multilayer Ohmic contacts to n-type GaN. *J. Appl. Phys.* **2003**, *93*, 1087. [CrossRef]
39. Hajlasz, M.; Donkers, J.J.T.M.; Sque, S.J.; Heil, S.B.S.; Gravesteijn, D.J.; Rietveld, F.J.R.; Schmitz, J. Sheet resistance under Ohmic contacts to AlGaN/GaN heterostructures. *J. Schmitz Appl. Phys. Lett.* **2014**, *104*, 242109. [CrossRef]
40. Lu, C.; Chen, H.; Lv, X.; Xie, X.; Mohammad, S.N. Temperature and doping-dependent resistivity of Ti/Au/Pd/Au multilayer ohmic contact to n-GaN. *J. Appl. Phys.* **2002**, *91*, 9218. [CrossRef]
41. Kim, H.; Ryou, K.J.; Dupuis, R.D.; Lee, S.-N.; Park, Y.; Jeon, J.-W.; Seong, T.-Y. Electrical characteristics of contacts to thin film N-polar n-type GaN. *Appl. Phys. Lett.* **2013**, *102*, 052107.

© 2019 by the authors. Licensee MDPI, Basel, Switzerland. This article is an open access article distributed under the terms and conditions of the Creative Commons Attribution (CC BY) license (http://creativecommons.org/licenses/by/4.0/).